Lecture 3. Low density environments, structure & dynamics

Diego Garcia Lambas, IATE - Observatorio Astrónomico. Córdoba Argentina.

Espirito Santo, September 2022

2dFGRS

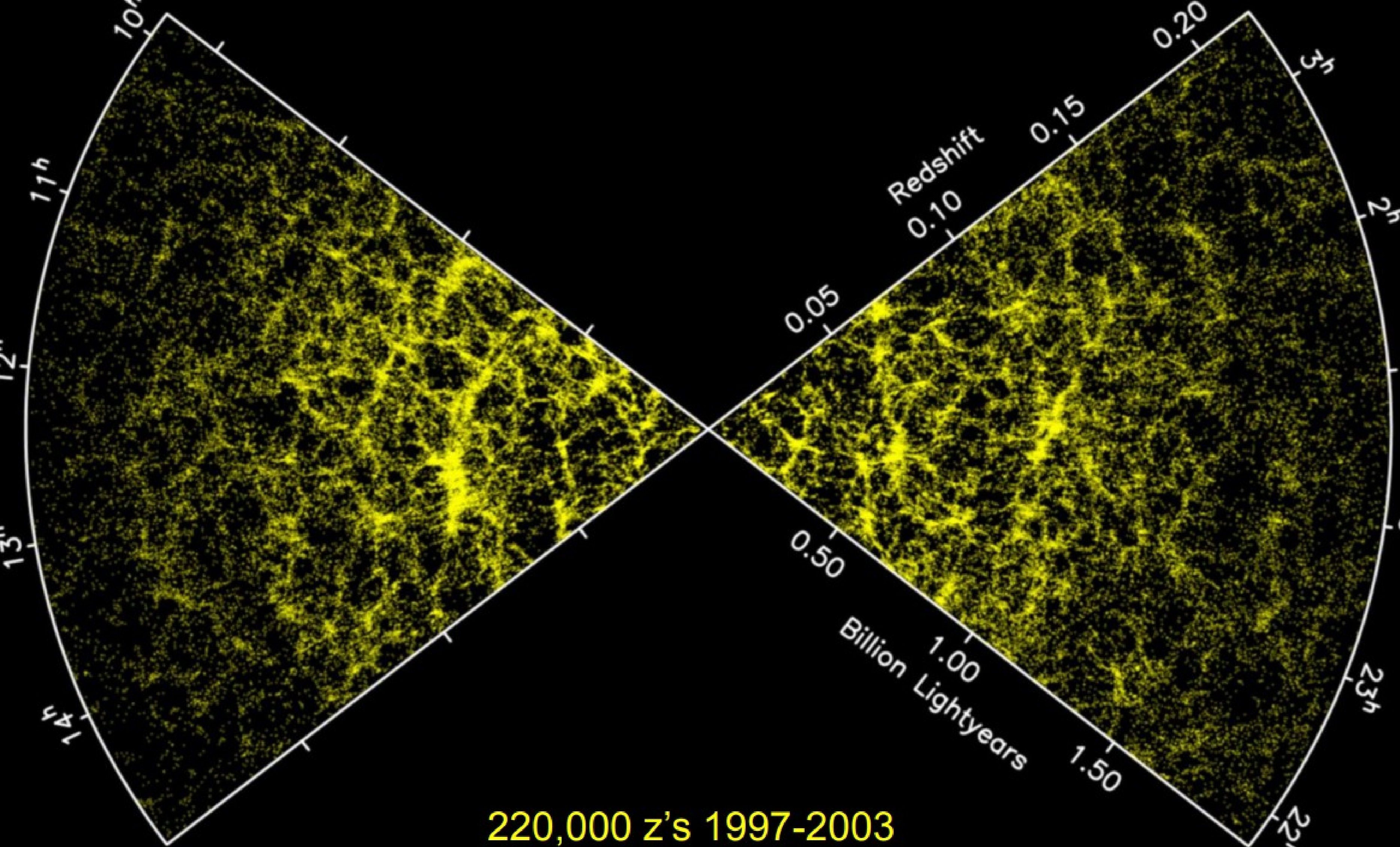

220,000 z's 1997-2003

1. *Voronoi tessellation.* A Voronoi tessellation is performed to obtain an estimation of the density field: each halo has an associated cell with volume $V_{\rm cell}$, and a density given by the inverse of that volume: $\rho_{\rm cell} = 1/V_{\rm cell}$. We used a parallel version of the public library VORO++ (Rycroft, 2009).

2. *Selection of candidates.* A first selection of underdense regions is done by selecting all Voronoi cells that satisfy the following criterion in local density contrast: $\delta_{\rm cell} < -0.7$. Each underdense cell is considered the centre of a potential void.

3. *Growth of spheres.* Centred on each candidate, the integrated density contrast, $\Delta(r)$, is computed in spheres of increasing radius r until the overall density contrast satisfies a redshift-dependent threshold of $\Delta_{\rm id}$, obtained from the spherical evolution model (Gunn; Gott III, 1972; Lilje; Lahav, 1991) by fixing a final spherical perturbation of $\Delta_{\rm id,0} = -0.9$ for $z = 0$.

4. *Optimisation.* Once these first void candidates are identified, step 3 is repeated, but now starting in a randomly displaced centre proportional to 0.25 times the radius of the candidate. Then, the void centre is updated to a new position if the new radius is larger than the previous one. This process is repeated iteratively until convergence to a sphere with maximum radius is achieved. We adopted the criterion that the optimal sphere is obtained if the algorithm can not find a bigger one during a lapse of 50 iterations. This normally takes between 200 and 300 iterations in total. In this way, this procedure mimics a random walk around the original centre in order to obtain the largest possible sphere in that local minimum of the density field.

5. *Overlap filtering.* Finally, the list of void candidates is cleaned so that each resulting sphere does not overlap with any other. This cleaning is done by ordering the list of candidates by size and starting from the largest one. The final result is a catalogue of non-overlapping spherical voids with a well-defined centre, a radius $R_{\rm v}$, and overall density contrast $\Delta(R_{\rm v}) = \Delta_{\rm id}$.

Cosmolgy with cosmic voids

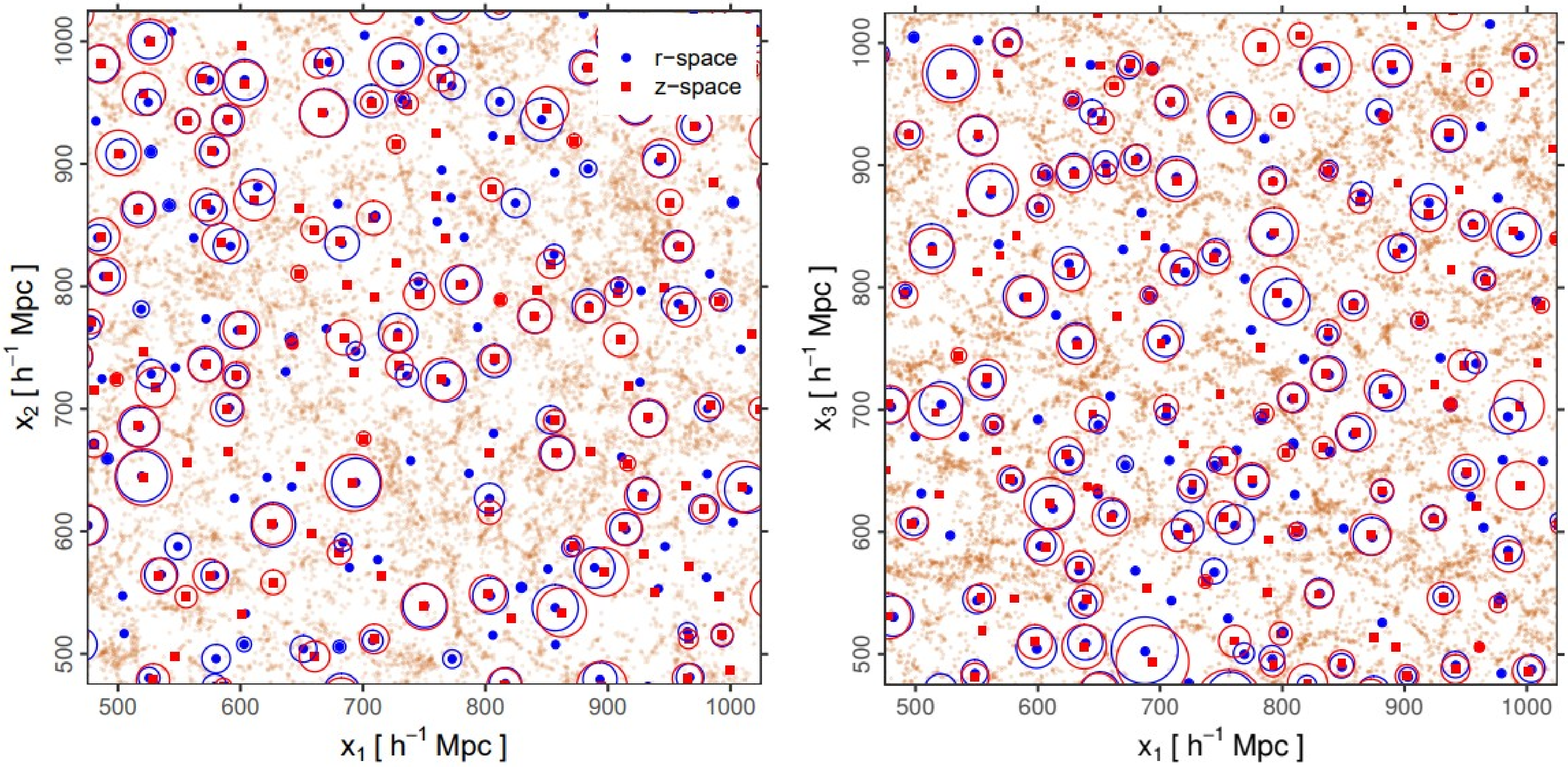

Figure 1. Slices of the Millennium XXL simulation box showing the distribution of haloes and voids from the TC samples of Table 1. Real-space void centres are represented with blue dots, whereas redshift-space centres, with red squares. Bijective voids, in turn, are represented with circles, the intersections of the spherical voids with the mid-plane of the slice. *Left panel.* Slice in the range $500 \leq x_1/h^{-1}\text{Mpc} \leq 1000$, $500 \leq x_2/h^{-1}\text{Mpc} \leq 1000$ and $95 \leq x_3/h^{-1}\text{Mpc} \leq 105$, a representation of the plane-of-sky distribution. *Right panel.* Slice in the range $500 \leq x_1/h^{-1}\text{Mpc} \leq 1000$, $95 \leq x_2/h^{-1}\text{Mpc} \leq 105$ and $500 \leq x_3/h^{-1}\text{Mpc} \leq 1000$, a representation of the line-of-sight distribution. Bijective voids span the same regions in both spaces. Voids expand and their centres shift when they are mapped from r-space into z-space.

Cosmic Voids

Sparkling Universe

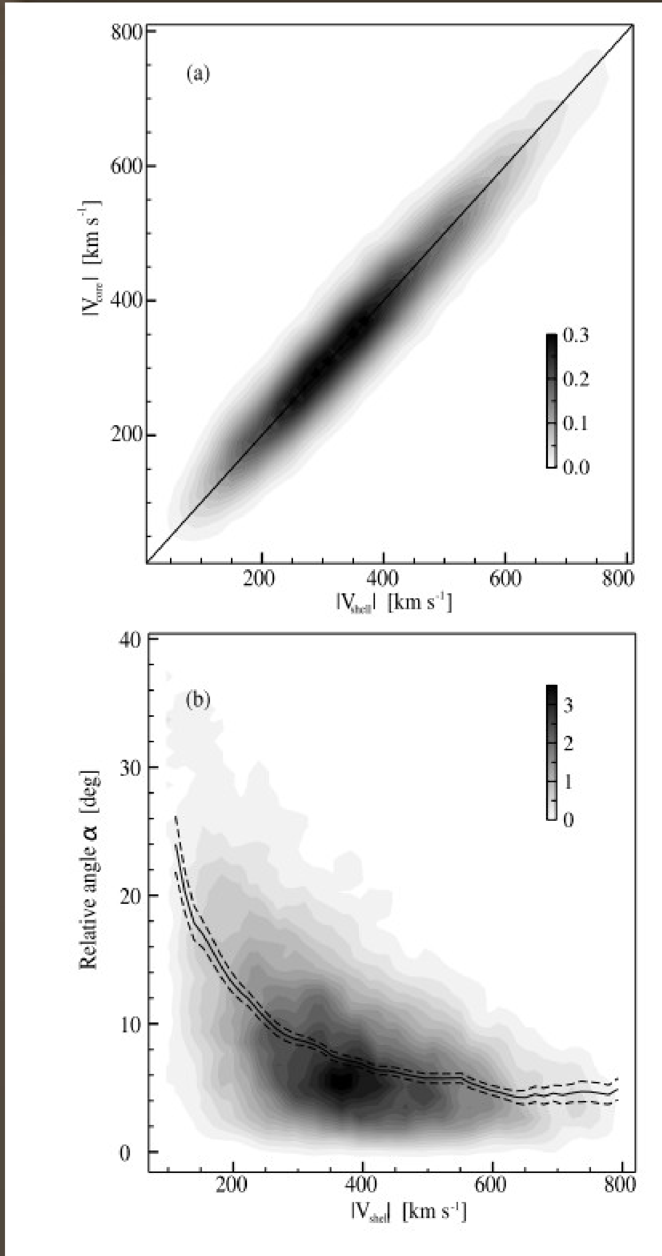

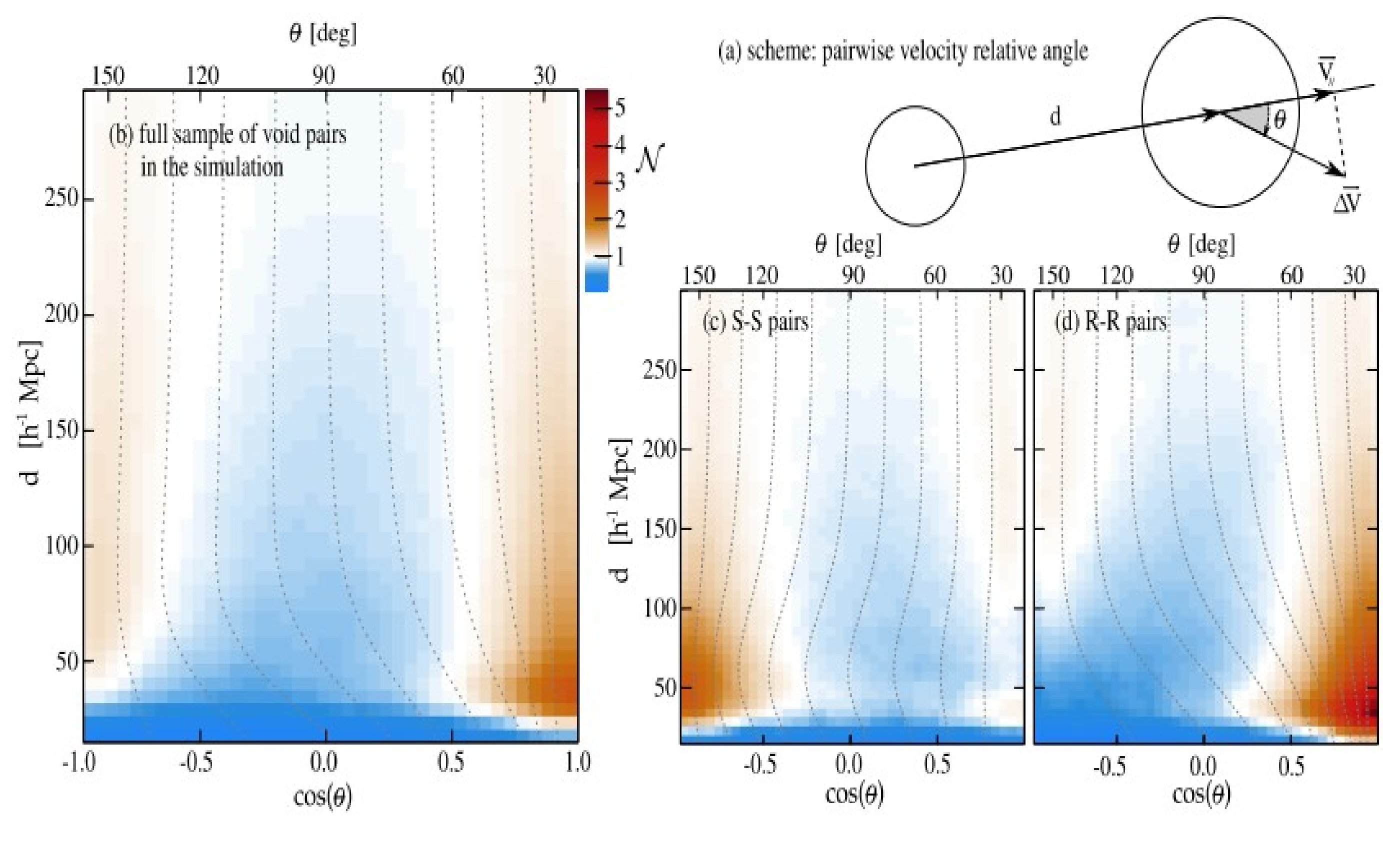

Figure 2. Coherence and bimodality of cosmic void relative motions. We show $\mathcal{N}$, the number counts of void pairs as a function of cos(θ) and separation, normalized to the expected number for a uniform distribution of voids without velocity coherence. The angle θ is that subtended by the void pairwise velocity ($\Delta\vec{V}$) and the void relative separation ($\Delta\vec{R}$), as portrayed in panel (a). Panel (b) shows the results for all void pairs, panels (c) and (d) correspond to S-S and R-R pairs, respectively. Dotted lines represent the deciles of the distribution of cos(θ).

Galaxies in cosmic voids different from elsewhere

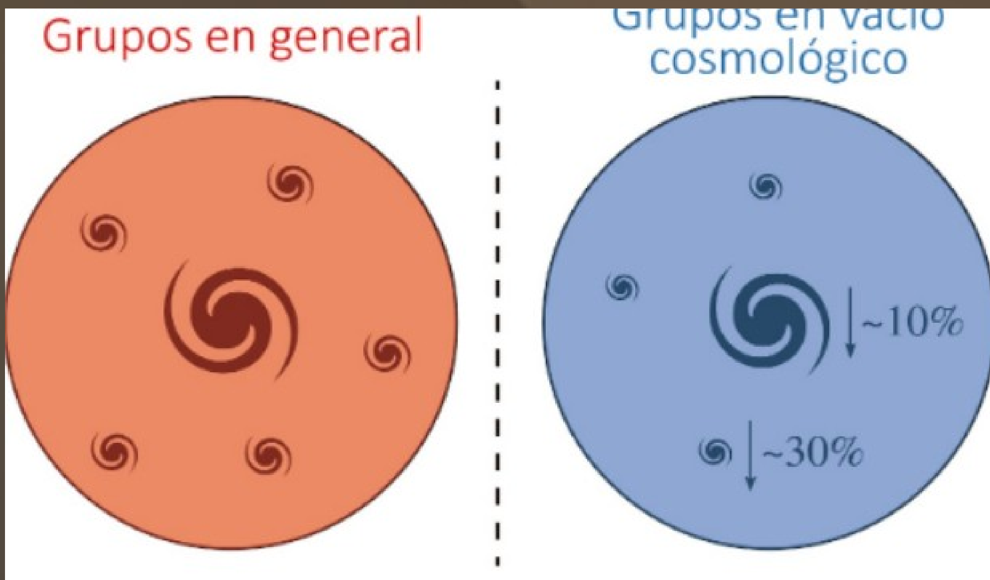

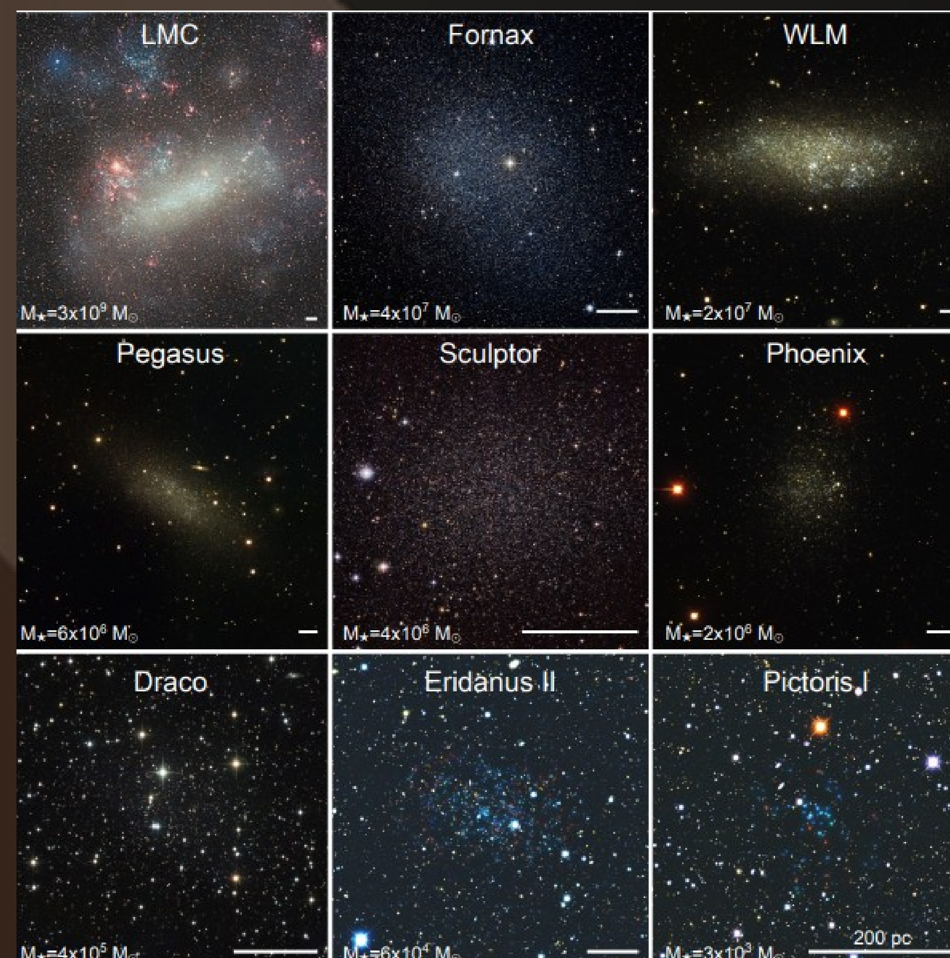

Dwarf galaxies , including extremely faint, almost devoid of stars, only studied in the Local Group.

Huge M/L ratios in extremely faint galaxies

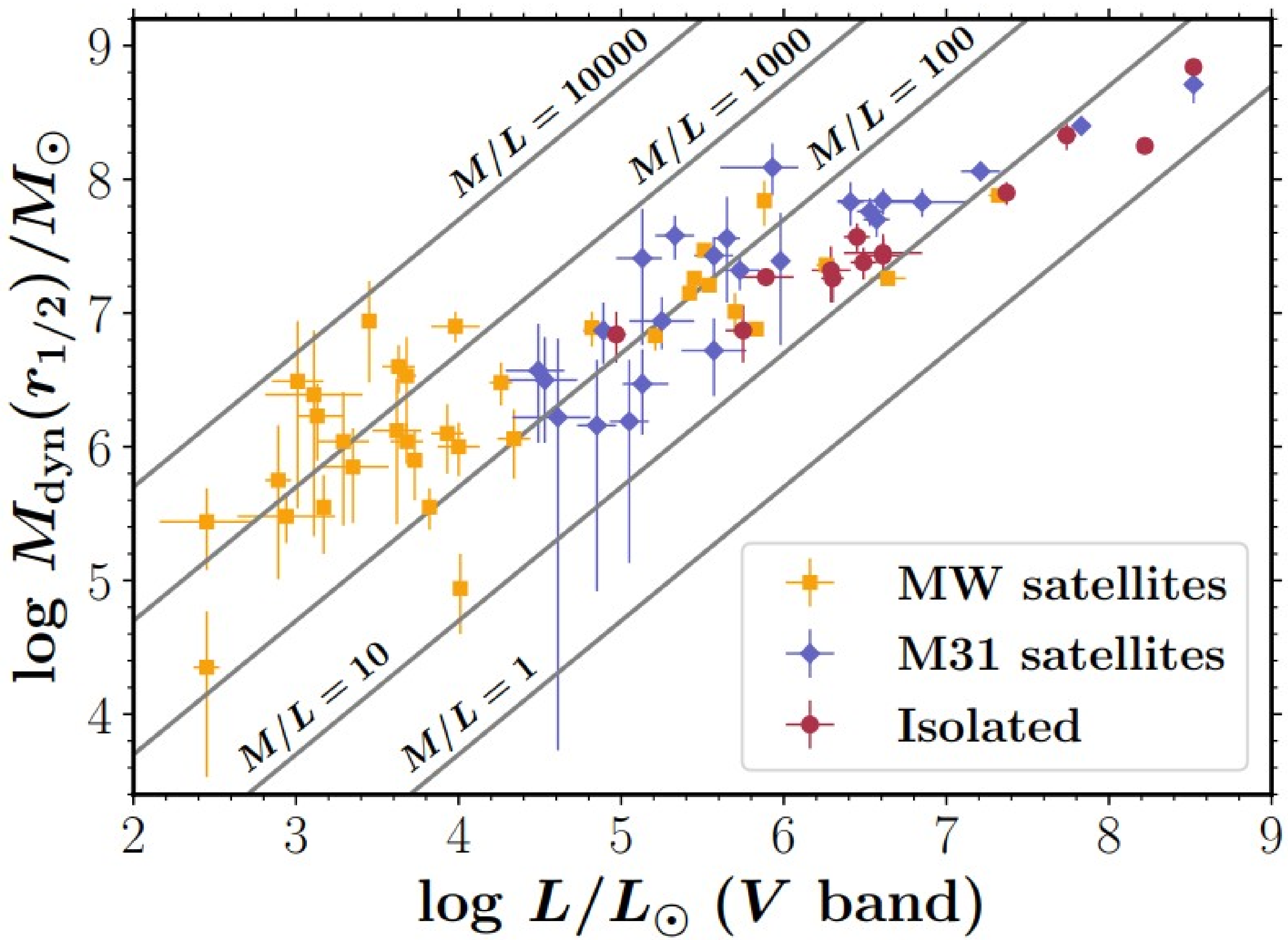

- Spin alignment of galaxies in voids. Cosmic voids as a source of galaxy rotation ?

Davila, Lares, DGL, 2022.

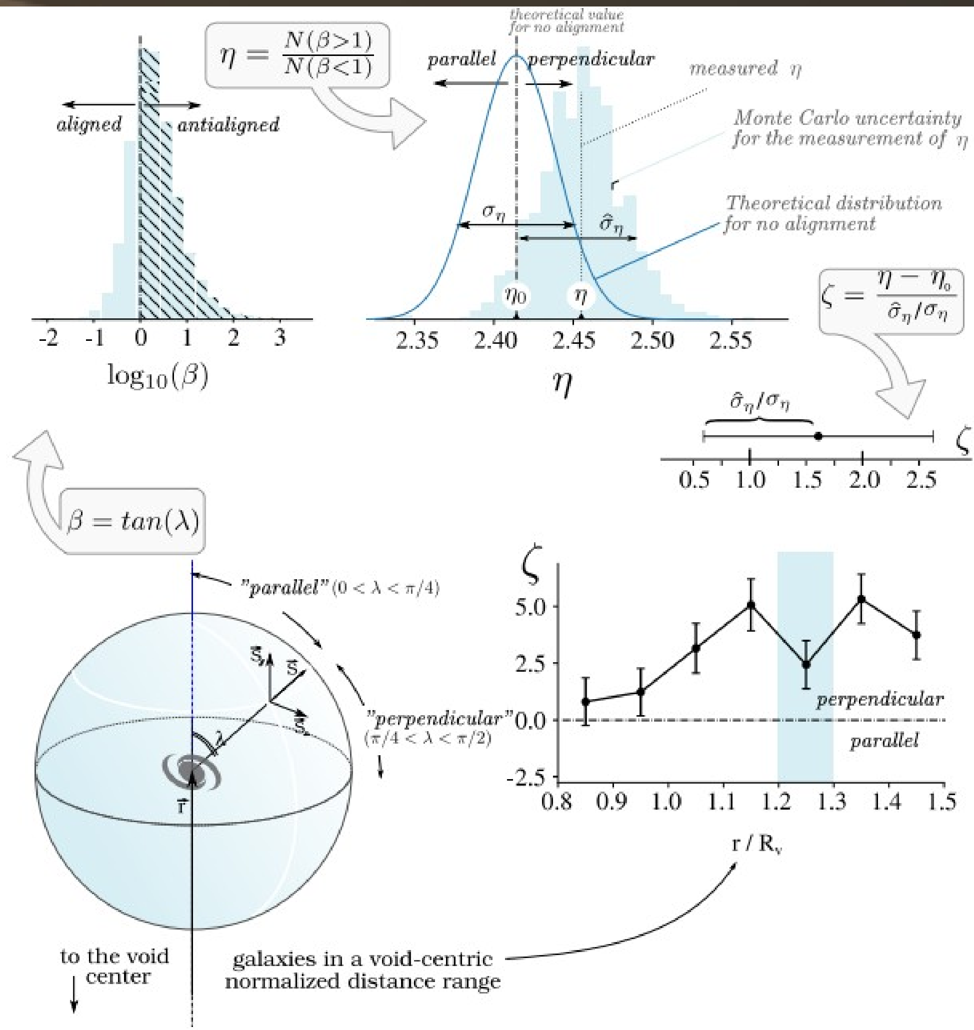

Figure 1. Scheme of the analysis performed in the search for alignment signals of galaxy discs around voids. We start with a λ parameter, the acute angle between the spin vector and the galaxy vector position w.r.t. the void center. Then the ratio of galaxies with $\tan(\lambda) > 1$ and with $\tan(\lambda) < 1$ is compared with a theoretical distribution for a randomly oriented galaxy sample for different bins in radial distance to the void center. Finally, a normalized parameter is defined, ζ, to show both the trend of alignment, if any, and its statistical significance; e.g. if $\zeta > 3$, then this population of galaxies shows a trend of being perpendicularly aligned with a confidence of over 3σ.

Voids as generators of galaxy angular momentum !

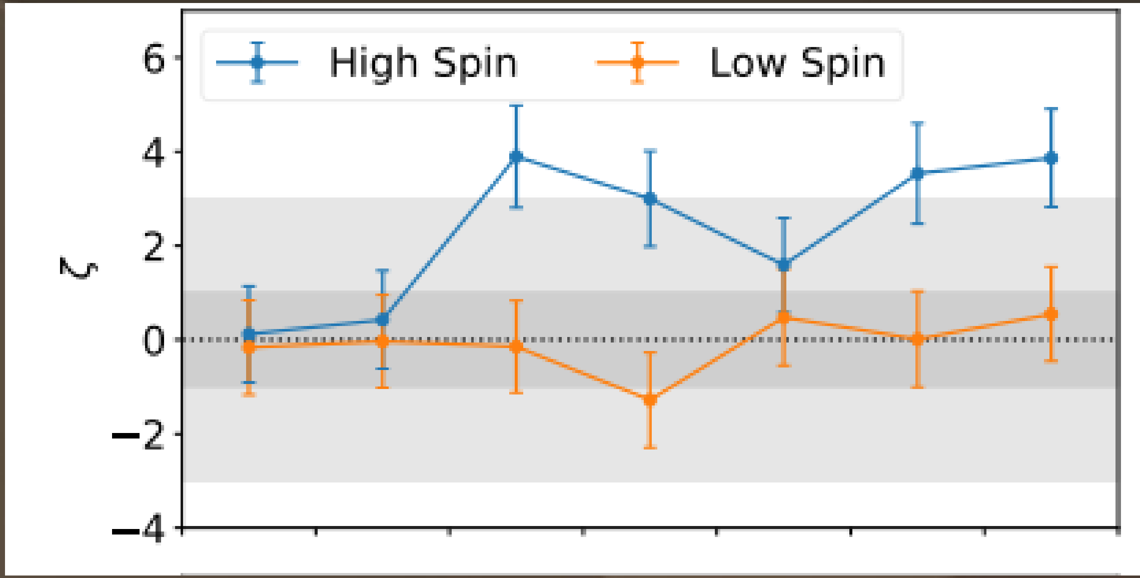
High Spin
Low Spin
6
4
2
0
−2
−4
ζ

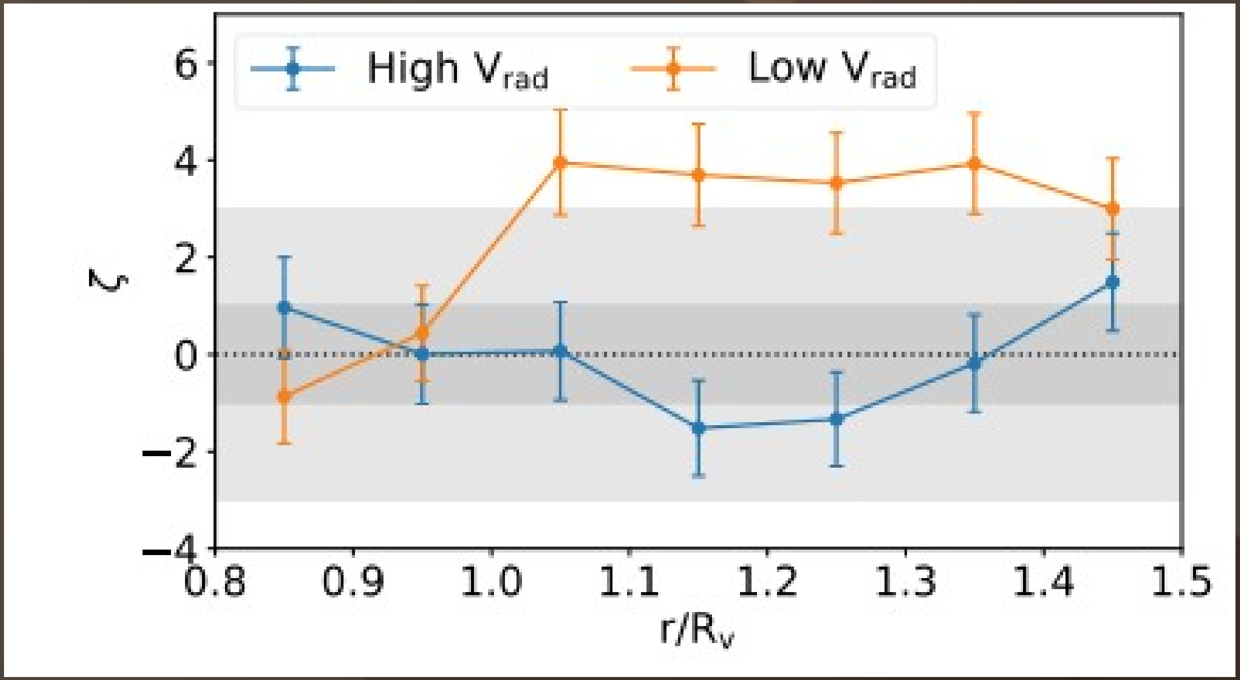
High V_{rad}
Low V_{rad}
6
4
2
0
−2
−4
ζ
0.8
0.9
1.0
1.1
1.2
1.3
1.4
1.5
r/R_v

- Dynamics of galaxies in low density regions: How cumply is the mass distribution in cosmic voids ? Are there dark massive galaxies inside ?

Alfaro, Ruiz , DGL. 2018.

Simulating void galaxies & comparison to observations

Correlation functions in redshift-space → pairwise velocities within Cosmic Voids.

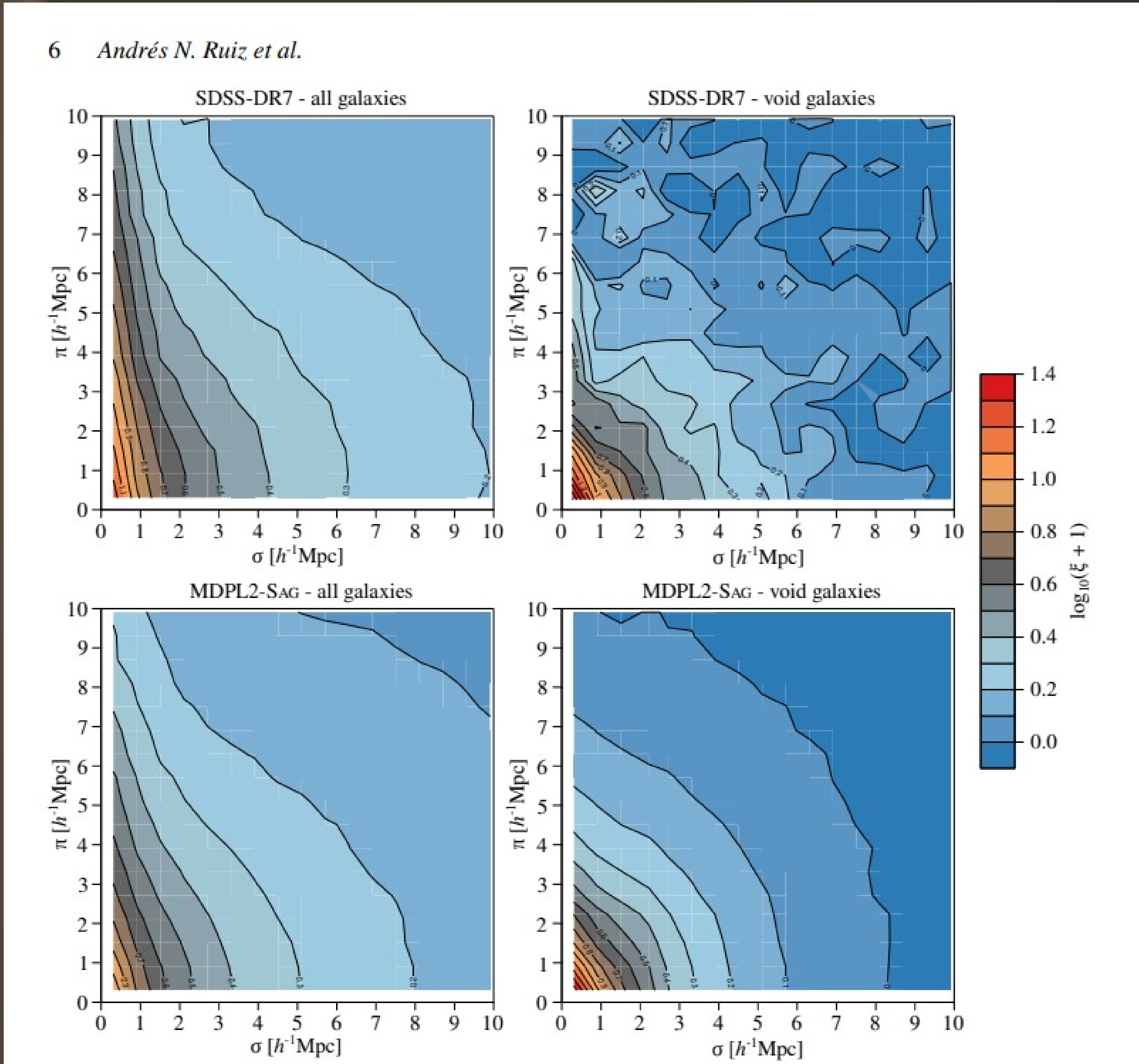

In simulations, the correlation functions within cosmic voids behave in a similar fashion than in the Data

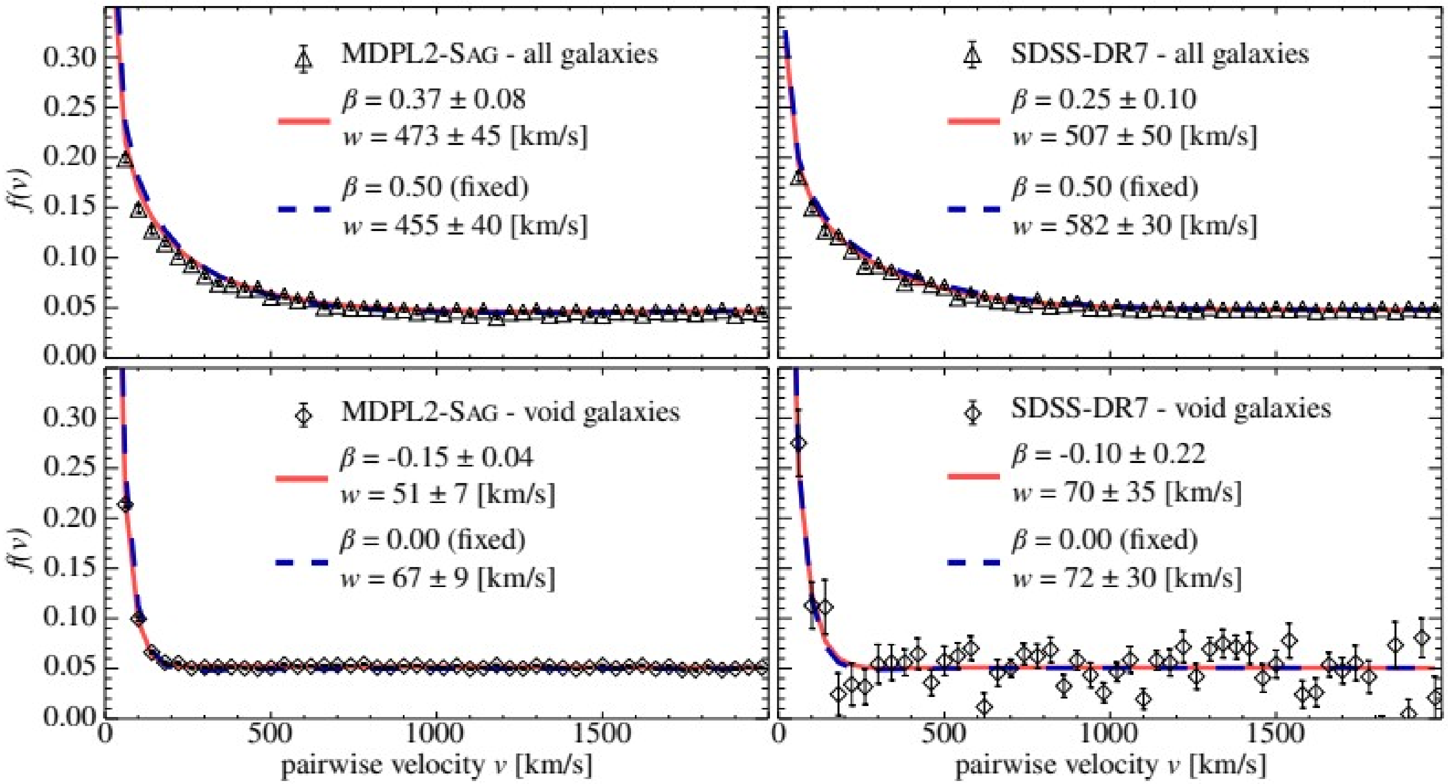

Figure 6. Measured and fitted pairwise velocity distributions. Upper panels correspond to all galaxies for MDPL2-SAG (left) and SDSS-DR7 (right). Bottom panels show the results for void galaxies for MDPL2-SAG (left) and SDSS-DR7 (right). The measured $f(v)$ is represented by triangles (all galaxies sample) and diamonds (void galaxies sample). Two model fits are shown: varying both β and w parameters in solid red lines and fixing β to a fiducial value and varying only w in dashed blue lines (see text for details). The values of the parameters β and w are shown in the respective key figures. Errorbars in measured points where estimated via the Jackknife resamplings of $\xi(\sigma, \pi)$.

Galaxies residing in Cosmic Voids have a mean pairwise velocity dispersion an order of magnitude lower than average

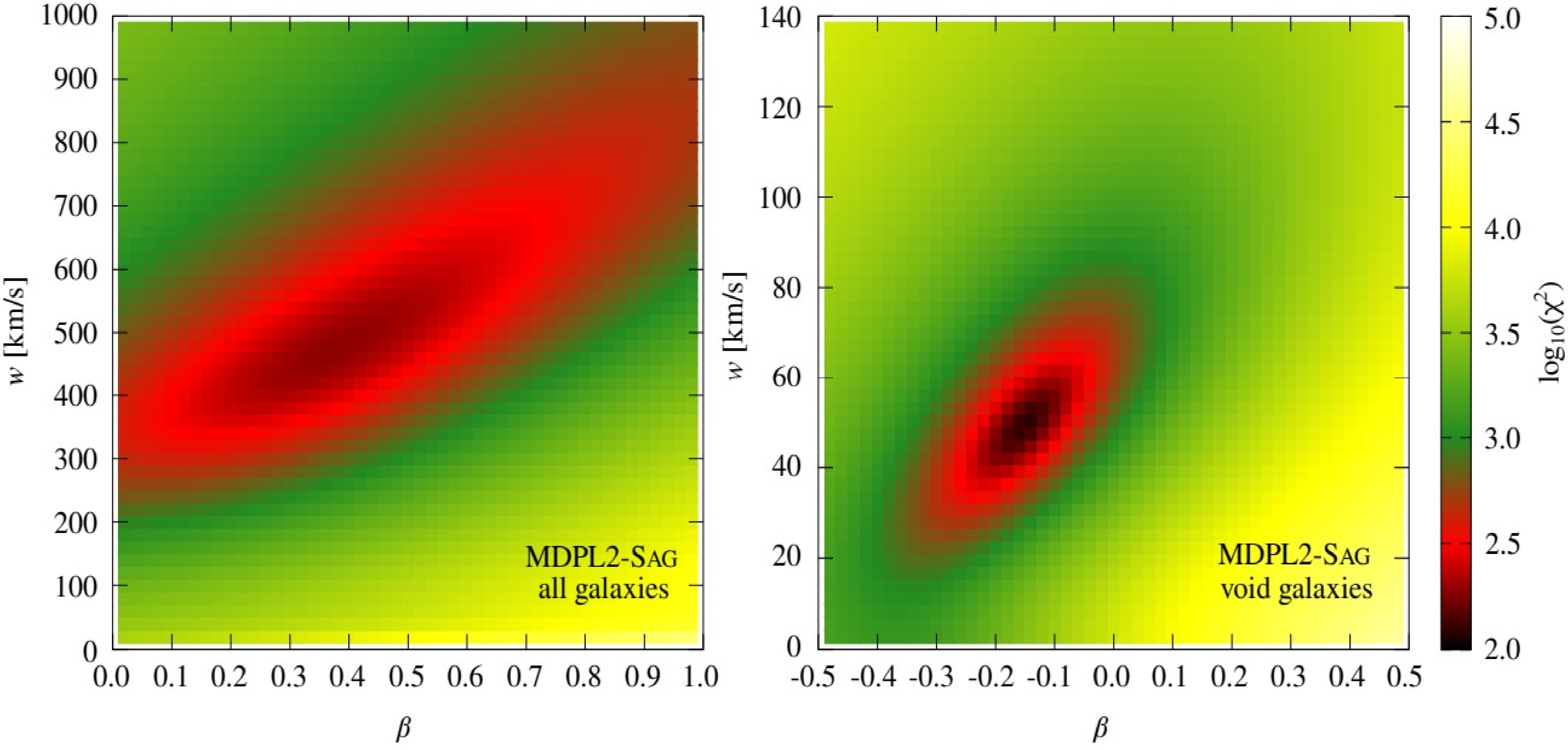

Figure 7. Maps of $\log_{10}(\chi^2)$ resulting from the fitting procedure, described in Sec. 4.3 to determine β and w for the case of all galaxies (left) and void galaxies (right) in the MDPL2-SAG catalogue.

Faint galaxy-structure interactions

Intergalaxtic gas in galaxies interact with filamentary structure: quenching in cosmic sheets. Pasha et al. 2022

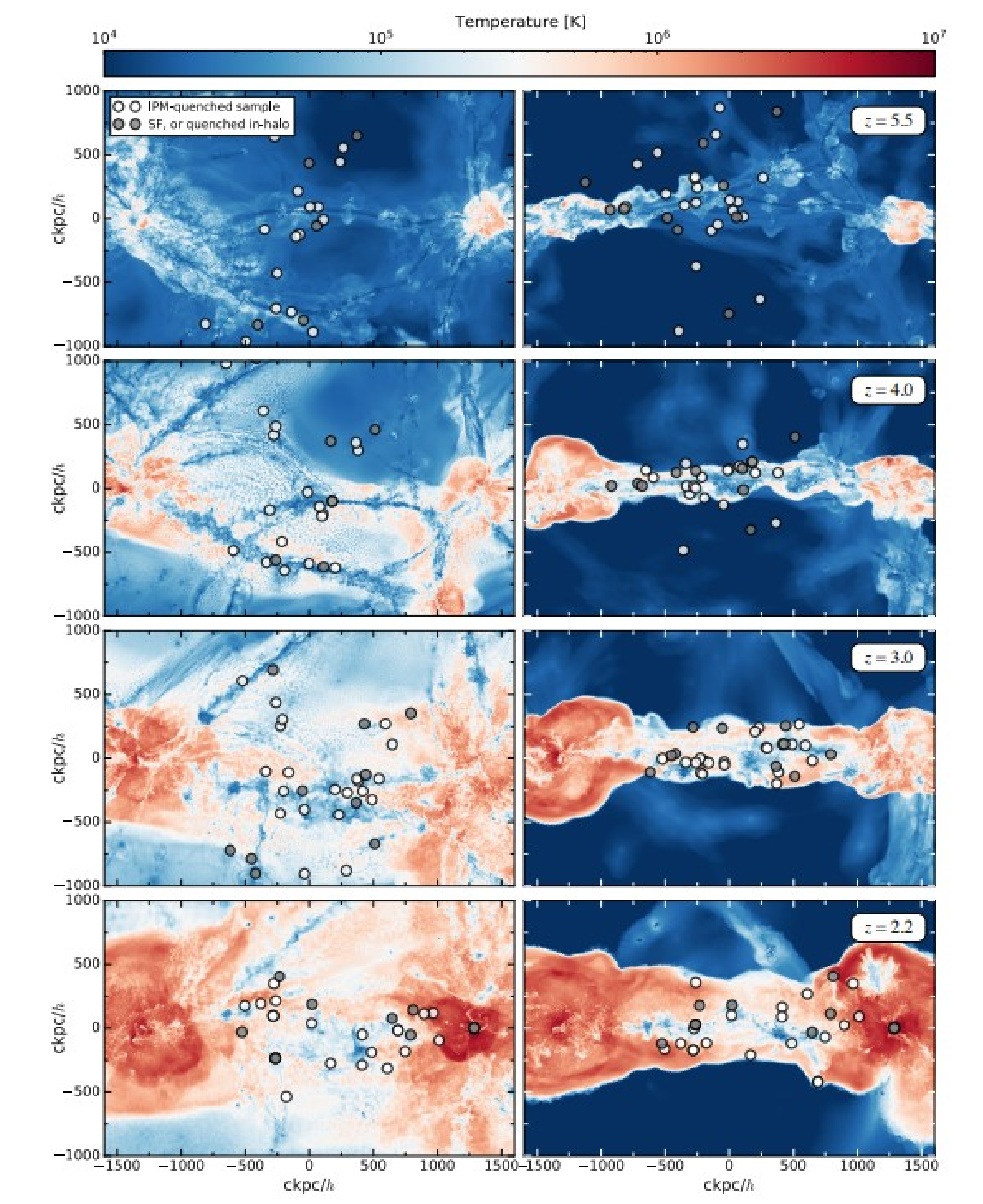

Figure 1. Face-on (left) and edge-on (right) views of the density-weighted temperature in the IPMSim simulation at 4 different redshifts, with an integration depth of 400 ckpc/h. Marked in all panels are the galaxies selected at $z = 3$ for analysis (see Section 2.2); cospatiality with the sheet at this redshift was a selection criterion, visible in the right hand panel. Points are colored by whether the given system quenches due to the accretion shock in the IPM (white) and those which either remain star forming, or quench within 3 R_v of the proto-clusters (grey).

Substructure in void shells and global dynamics

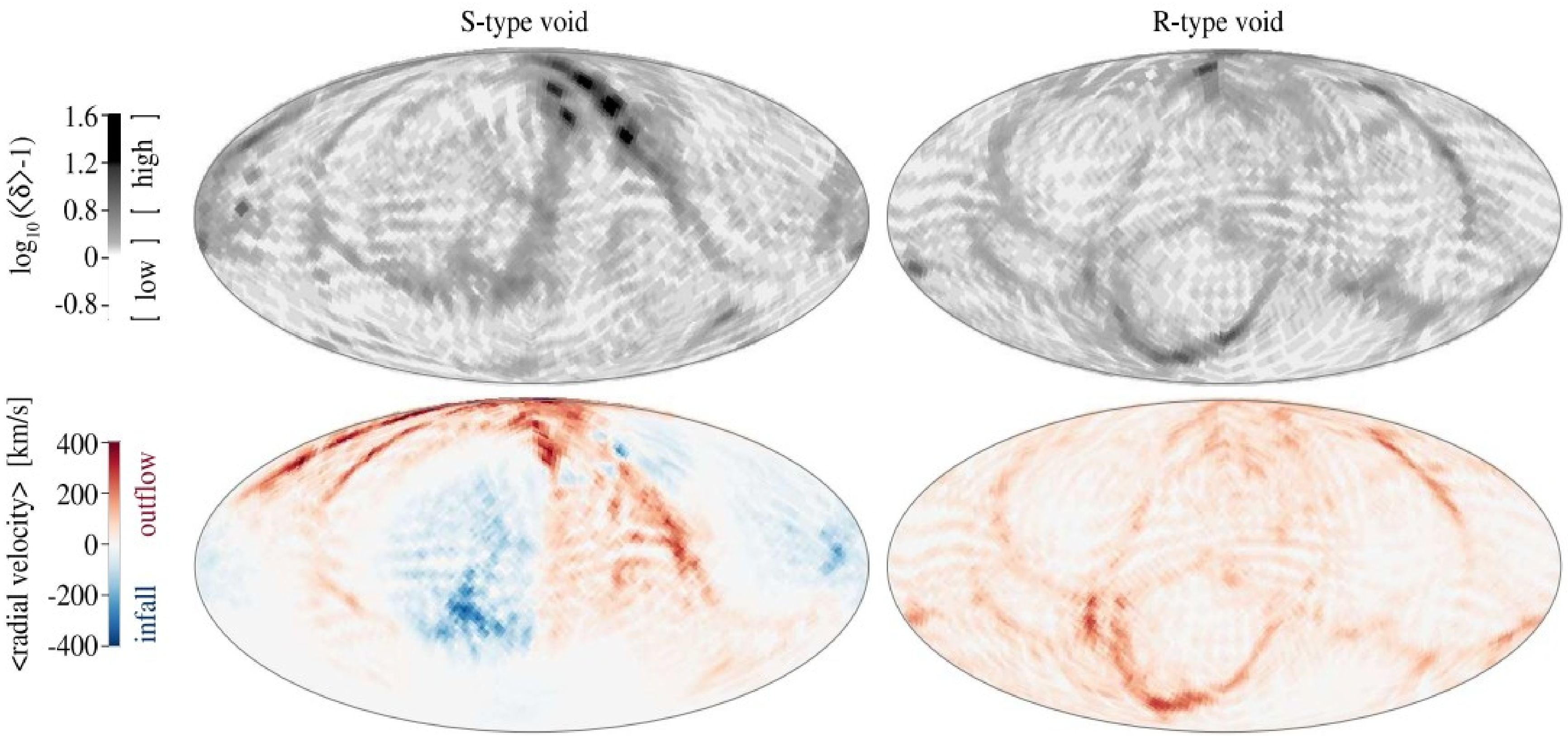

Figure 1. Mollweide projection of mass density contrast (top panels) and radial velocity (bottom panels) pixel maps of two voids with the utmost S ("void–in–cloud", left panels) or R-type ("void–in–void", right panels) behaviour. All simulation particles in the range $0.9 < r/R_{\rm void} < 1.1$ are used to compute averaged values within each pixel. The two voids shown in this Figure have been chosen so that they show the greatest separation in the void classification scheme, based on the integrated density profiles (detailed in Paper I). This two cases exemplify how the structure of the velocity field in the inner parts of a void at 1 void radius exhibits very distinct behaviour depending on their environment (defined around 3 void radius, i.e. R- or S-type void). Such differences are not expected in linear theory, given that both regions by definition enclose the same amount of integrated overdensity $\Delta(R_{\rm void}) = -0.9$.

Substructure in void shells and global dynamics → topology of low/high velocity structures in void shells and its relation to galaxy spins

Void-galaxy cross correlation function

$$1 + \xi(\sigma, \pi) = \int d^3w \, g(\boldsymbol{r}, \boldsymbol{w}) \, [1 + \xi(r)] \, ,$$

$$\sigma = \sqrt{r_1^2 + r_2^2} \text{ and } \pi = r_3 + w_3/\mathrm{H},$$

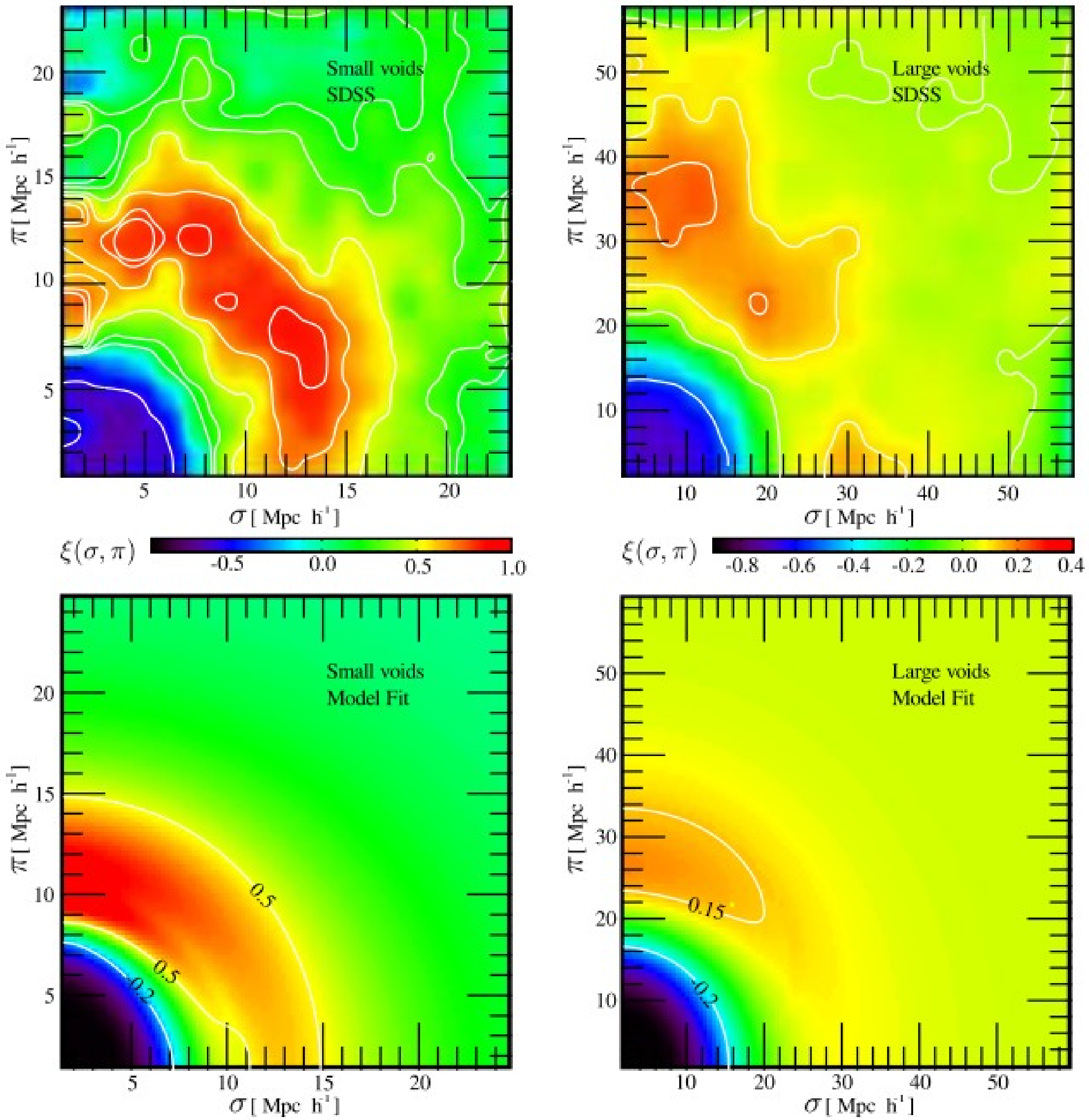

Figure 1. Redshift space distortions of galaxies in the SDSS (upper panels) and the best fit models (bottom panels) for small S-type voids in S1 ($6 < R_{void}/h^{-1}$ Mpc< 8, left panels) and large R-type voids in S3 ($10 < R_{void}/h^{-1}$ Mpc< 20, right panels). The fractions of small R-type voids and large S-type voids are 0.3 and 0.1, respectively. Notice that spatial and color scales change for small and large voids.

$$1+\xi(\sigma,\pi)=\int dw_3\frac{1}{\sqrt{2\pi}\sigma_v}\exp\left(\frac{-\left(w_3-v(r)\frac{r_3}{r}\right)^2}{2\sigma_v}\right)[1+\xi(r)]$$

where $r_3=\pi-w_3/\mathrm{H}$ and $r^2=\sigma^2+\left(\pi^2-\frac{w_3}{\mathrm{H}}\right)^2$.

$$v(r)\approx-\mathrm{H}r\Delta(r)\frac{\Omega_m^{0.6}}{3}$$

$$\xi(r)=\frac{1}{3r^2}\frac{\mathrm{d}}{\mathrm{d}r}\left(r^3\Delta(r)\right).$$

$$1+\xi^{s}(\sigma,\pi)=\int_{-\infty}^{\infty}[1+\xi(r)]\frac{1}{\sqrt{2\hat{\pi}}\sigma_{\rm v}}\exp\left[-\frac{(v_{\parallel}-v(r)\frac{r_{\parallel}}{r})^{2}}{2\sigma_{\rm v}^{2}}\right]{\rm d}v_{\parallel}$$

Cosmolgy with cosmic voids

Void size function: redshift space distortions/AP effect

Void motions

https://arxiv.org/pdf/2007.12064.pdf
https://arxiv.org/pdf/2007.12064.pdf

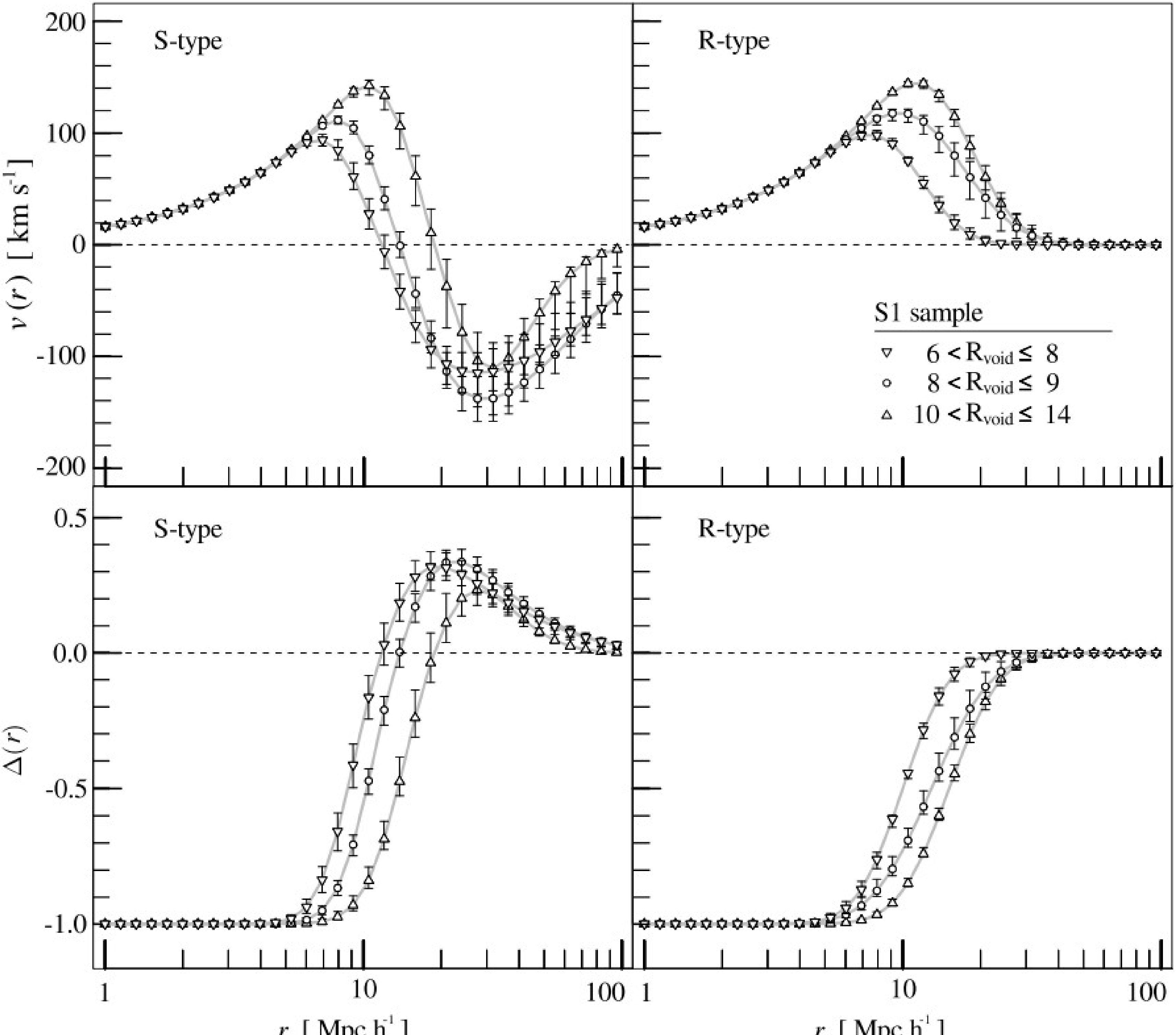

S-type
R-type
S-type
R-type
S1 sample
6 < R_void ≤ 8
8 < R_void ≤ 9
10 < R_void ≤ 14
v(r) [km s^-1]
Δ(r)
r [Mpc h^-1]
r [Mpc h^-1]
200
100
0
-100
-200
0.5
0.0
-0.5
-1.0
1
10
100
1
10
100

$$\Delta_{\mathrm{R}}(r) = \frac{1}{2}[\mathrm{erf}(S\log_{10}(r/R)) - 1].$$

$$\Delta_{\mathrm{S}}(r) = \frac{1}{2}[\mathrm{erf}(S\log_{10}(r/R)) - 1] + P\exp\left[-\frac{\log_{10}^2(r/R)}{2\Theta^2(r)}\right],$$

$$\Theta(r) := \begin{cases} 1/\sqrt{2S} \text{ if } r < R \\ 1/\sqrt{2W} \text{ if } r > R. \end{cases}$$

Expansion velocity

- Linear model for expansion velocity

$$v(r) = -\frac{1}{3}\frac{H(z)}{(1+z)}\beta(z) r \Delta(r).$$

AP effect: testing geometry of the universe with voids

$$v(r) = -\frac{1}{3}\frac{H(z)}{(1+z)}\beta(z)r\Delta(r),$$

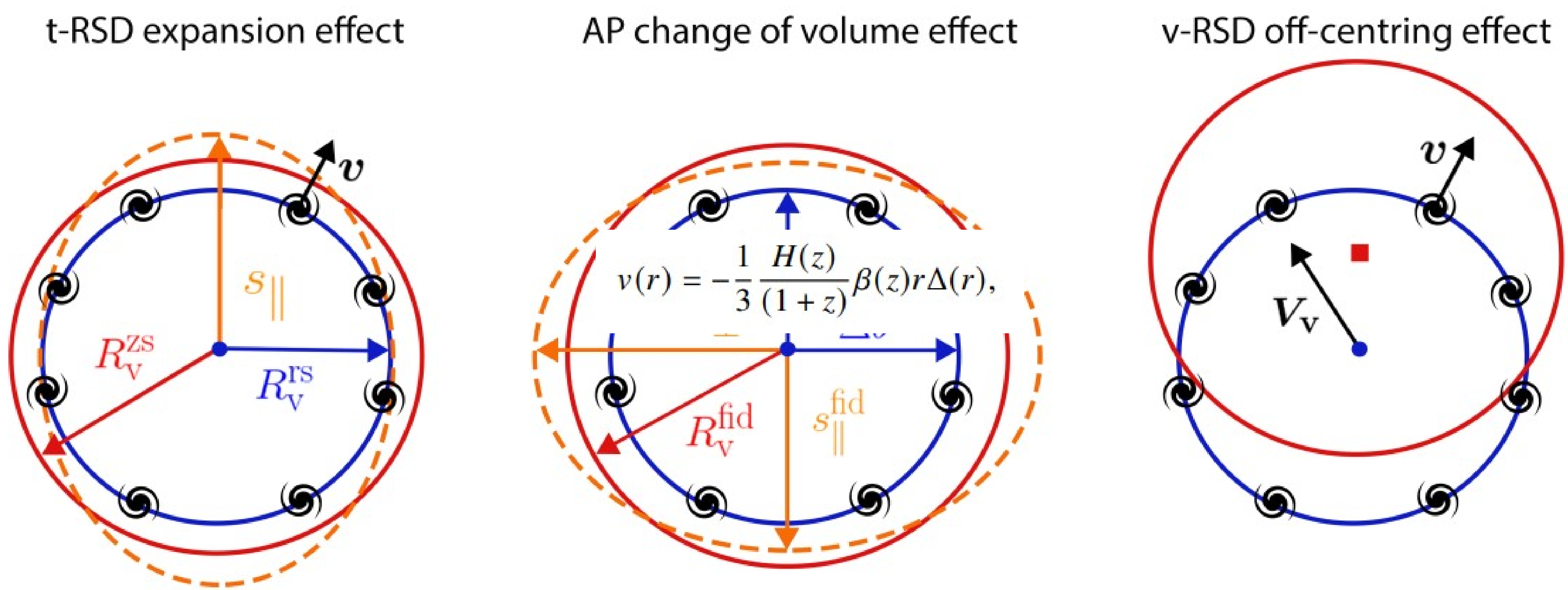

Figure 3. Schematic illustration of the three z-space effects in voids. In all panels, a hypothetical spherical r-space void of radius R_V^{rs} is represented with a blue solid circle with some galaxies. The LOS direction is vertical. *Left panel. Expansion effect.* The r-space void appears elongated along the LOS in z-space with LOS semi-axis $s_{\|}$ (orange dashed ellipse). The void finder identifies an equivalent sphere of radius R_V^{zs} (red solid circle). This effect is a by-product of tracer dynamics at scales around the void radius (t-RSD). *Middle panel. AP change of volume.* The r-space void is distorted into an ellipsoid with LOS semi-axis $s_{\|}^{fid}$ and POS semi-axis $s_{\perp}^{fid}$ (orange dashed ellipse). The void finder identifies an equivalent sphere of radius R_V^{fid} (red solid circle). This is a geometrical effect caused by the selection of a fiducial cosmology in order to transform the observable dimensions of the void, an angular radius $\Delta\theta$ and a redshift radius Δz, into a Mpc-scale (no t-RSD are included here for a better comprehension). *Right panel. Off-centring effect.* The r-space void centre appears shifted along the LOS in z-space. This effect is a by-product of void dynamics (v-RSD), i.e. the global dynamics of the whole region containing the void. The three effects can be treated independently.

Distortions of void volume due to AP and RSD effects

$$R_{\mathrm{v}}^{\mathrm{zs}} = q_{\mathrm{AP}}\, q_{\mathrm{RSD}}\, R_{\mathrm{v}}^{\mathrm{rs}}.$$

POS and LOS Void-gx cross correlations

Correa et al. 2022

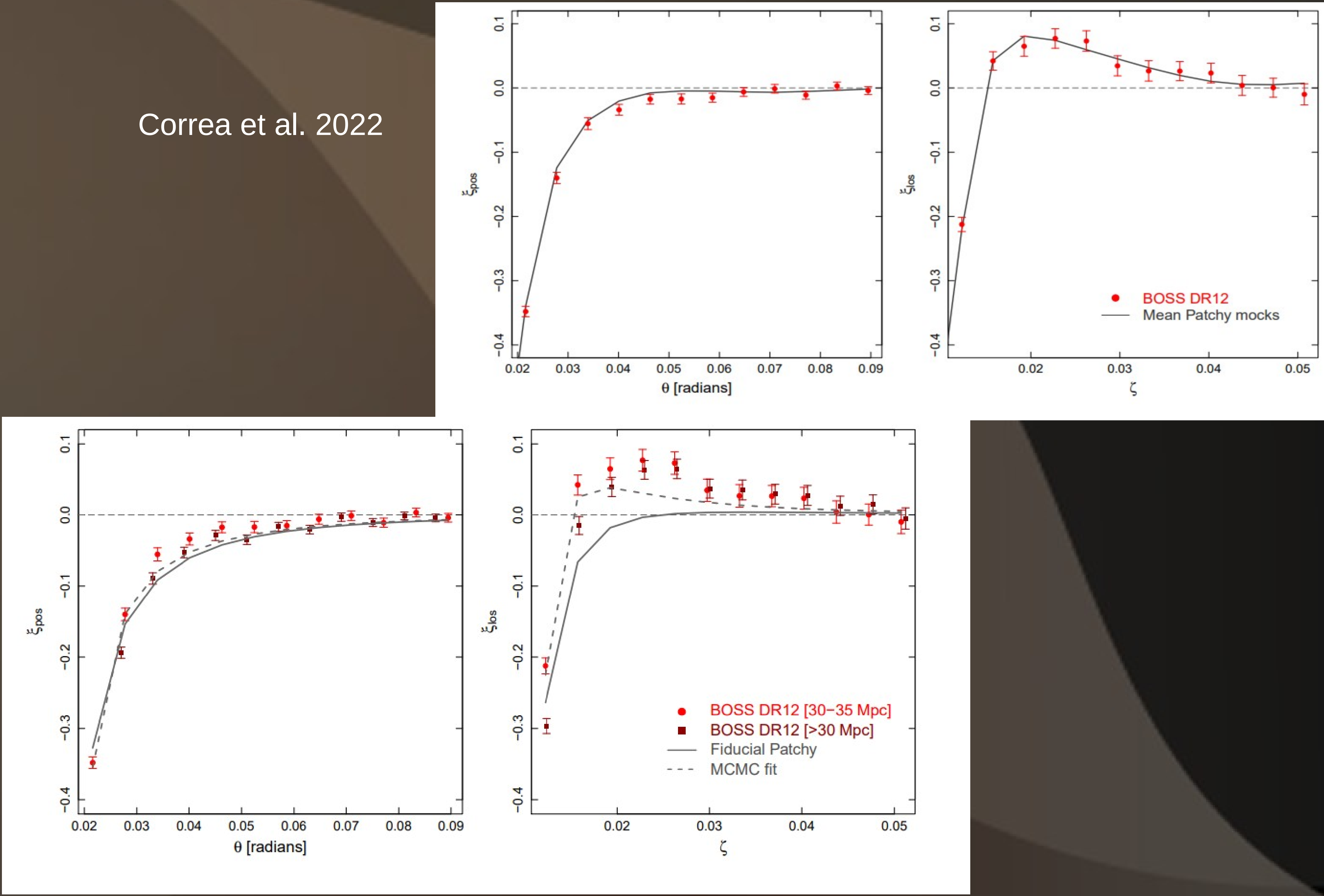

As a summary:

- Cosmic voids are simple structures with lot of potential for LSS studies
- Cosmogy using CV
- Internal dynamics
- Dwarf galaxies residing in CV / Dark matter

As a summary:

- Shell structures
- interesting relations between galaxy spins and void expansion
- Several tests for LCDM may be awaiting here !

- Obrigado !!